Chemical Science

ROYAL SOCIETY OF CHEMISTRY

EDGE ARTICLE

View Article Online
View Journal | View Issue

Check for updates

Cite this: *Chem. Sci.*, 2023, **14**, 8552

All publication charges for this article have been paid for by the Royal Society of Chemistry

Open Access Article. Published on 14 July 2023. Downloaded on 2/13/2026 6:50:17 PM. This article is licensed under a Creative Commons Attribution-NonCommercial 3.0 Unported Licence.

Sequence-controlled alternating block polychalcogenophenes: synthesis, structural characterization, molecular properties, and transistors for bromine detection†

Kuo-Hsiu Huang,[a] Huai-Hsuan Liu,[a] Kuang-Yi Cheng,[a] Chia-Lin Tsai[a] and Yen-Ju Cheng *[ab]

Sequence-controlled polychalcogenophenes have attracted much interest in terms of synthesis, structure and function in polymer science. For the first time, we developed a new class of alternating block conjugated copolymers denoted as poly(*alt*-AB)$_x$-*b*-(*alt*-AC)$_y$ where both blocks are constituted by an alternating copolymer. 3-Hexylthiophene (S), 3-hexylselenophene (Se) and 3-hexyltellurophene (Te) are used as A, B and C units to assemble three sequence-controlled polychalcogenophenes **P(SSe)*b*(STe)**, **P(SSe)*b*(SeTe)** and **P(STe)*b*(SeTe)** which are prepared by adding two different Grignard monomers in sequence to carry out Ni(dppp)Cl$_2$-catalyzed Kumada polymerization. The molecular weight, dispersity, and length of each block ($x = y$) and main-chain sequence can be synthetically controlled *via* the catalyst transfer polycondensation mechanism. The polymer structures, *i.e.* alternating block main chain with high side-chain regioregularity, are unambiguously confirmed by ^{1}H-NMR and ^{13}C-NMR. The optical and electrochemical properties of the polymers can be systematically fine-tuned by the composition and ratio of the chalcogenophenes. From GIWAXS measurements, all the polymers exhibited predominantly edge-on orientations, indicating that the packing behaviors of the alternating block polychalcogenophenes with high regioregularity are inherited from the highly crystalline **P3HT**. **P(SSe)*b*(STe)** exhibited a hole OFET mobility of 1.4×10^{-2} cm^2 V^{-1} s^{-1}, which represents one of the highest values among the tellurophene-containing polychalcogenophenes. The tellurophene units in the polymers can undergo Br_2 addition to form the oxidized **TeBr$_2$** species which results in dramatically red-shifted absorption due to the alternating arrangement to induce strong charge transfer character. The OFET devices using the tellurophene-containing polychalcogenophenes can be applied for Br_2 detection, showing high sensitivity, selectivity and reversibility.

Received 5th May 2023
Accepted 13th July 2023

DOI: 10.1039/d3sc02289g

rsc.li/chemical-science

Introduction

Biopolymers with perfectly ordered sequences exhibit unique structural properties and fascinating functions unmatched by synthetic polymers. The recent advances in organometallic chemistry in organic synthesis have paved the way to access various types of sequence-controlled polymers with novel structural features.[1–3] The synthesis of sequence-controlled conjugated polymers (SCCPs) is one of the emerging and challenging topics in polymer science.[4–9] SCCPs with structural regularity are prone to self-assembly into ordered nanostructures, which is essential for realizing high-performance organic optoelectronics, such as organic photovoltaics (OPVs)[10,11] and field-effect transistors (OFETs).[12,13] Regioregular poly(3-alkylthiophene) (P3AT) is one of the most representative semiconducting polymers widely applied in various organic optoelectronics due to its high crystallinity, ordered packing structure in thin film and good chemical stability.[14,15] However, the limited absorption window of 300 to 550 nm with fixed energy levels is the main deficiency of P3ATs. Despite the fact that aliphatic side-chain modification has been implemented to tailor the solubility and morphological properties of P3AT, it has little effect on the optical and electrochemical properties. Consequently, donor–acceptor (D–A) conjugated copolymers prepared by metal-catalyzed polymerization of an electron-deficient monomer with an electron-rich monomer have been considerably developed to tailor HOMO/LUMO energy levels with a tunable optical bandgap.[16,17] Nevertheless, incorporation of two discrepant units with different sizes, geometric shapes, polarities and side-chain substituents dramatically alters the intermolecular interactions, resulting in unpredictable solid-state molecular packing and morphology.

[a]*Department of Applied Chemistry, National Yang Ming Chiao Tung University, 1001 University Road, Hsinchu, 30010, Taiwan, China. E-mail: yjcheng@nycu.edu.tw*
[b]*Center for Emergent Functional Matter Science, National Chiao Tung University, 1001 University Road, Hsinchu, 30010, Taiwan, China*

† Electronic supplementary information (ESI) available. See DOI: https://doi.org/10.1039/d3sc02289g

© 2023 The Author(s). Published by the Royal Society of Chemistry

Open Access Article. Published on 14 July 2023. Downloaded on 2/13/2026 6:50:17 PM.
This article is licensed under a Creative Commons Attribution-NonCommercial 3.0 Unported Licence.

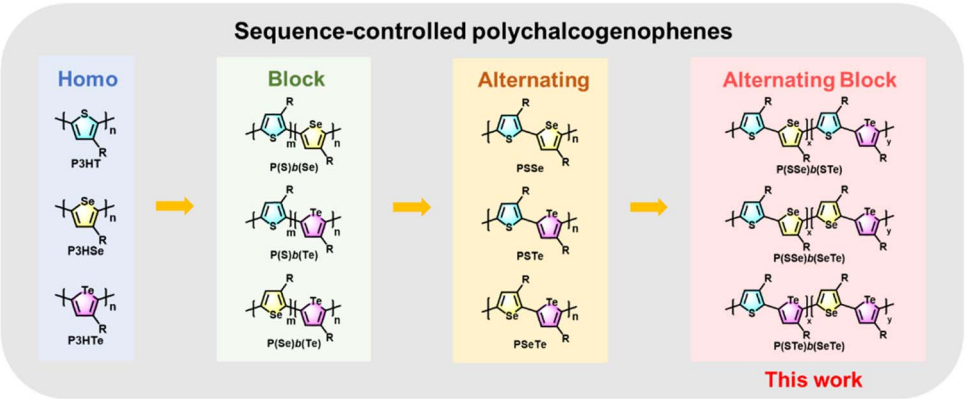

Fig. 1 Homopolychalcogenophenes **P3HT**, **P3HSe**, and **P3HTe**; block polychalcogenophenes **P(S)*b*(Se)**, **P(S)*b*(Te)** and **P(Se)*b*(Te)**; alternating polychalcogenophenes **PSSe**, **PSTe**, and **PSeTe**; and alternating block polychalcogenophenes **P(SSe)*b*(STe)**, **P(SSe)*b*(SeTe)**, and **P(STe)*b*(SeTe)** in this work.

Selenophene and tellurophene in the chalcogenophene family using heavier selenium and tellurium elements in group 16 have similar structural geometries to thiophene but different electronic properties.[18,19] Compared to thiophene, selenophene and tellurophene have lower aromaticity and higher polarizability resulting in a reduced HOMO/LUMO bandgap and enhanced intermolecular interactions.[20–27] Tellurophene has even more distinct properties and pronounced impacts due to the metalloid character of tellurium.[28,29]

Poly(3-hexylselenophene) **P3HSe** and poly(3-hexyltellurophene) **P3HTe** have been synthesized by using traditional catalyst transfer polymerization (CTP).[30–32] The strong intermolecular interactions of **P3HSe**, especially **P3HTe**, were found to unfavorably lead to reduced solubility, thereby limiting the molecular weight growth during polymerization and deteriorating the thin-film formation directly related to the charge transport, unless the high-carbon aliphatic side chains are introduced.[33]

It is envisaged that integration of selenophene or tellurophene analogs with thiophene in a polymer backbone provides a practical and effective approach to fine-tune optical and electronic properties without substantially altering the ordered packing behavior and sacrificing solution processability. Consequently, the assembling 3-hexylthiophene, 3-hexylselenophene and 3-hexyltellurophene monomers with controlled sequence, ratio, combination and regioregularity will lead to a new class of structurally and functionally appealing polychalcogenophenes.

Block copolymers with controlled morphology are of great significance in nanomaterials and nanotechnology.[34–37] Block polychalcogenophenes such as poly(3-hexylthiophene-*block*-3-hexylselenophene) **P(S)*b*(Se)** [38–43] and poly(3-hexylthiophene-*block*-3-hexyltellurophene) **P(S)*b*(Te)** [44] have been synthesized by controlling the addition sequence of the two monomers during the CTP process (Fig. 1).

On the other hand, synthesis of AB-type alternating polychalcogenophenes with high side-chain regioregularity is more challenging.[45–47] Recently, we developed a new series of well-designed AB-type monomers for the preparation of poly(3-hexylthiophene-*alt*-3-hexylselenophene) **PSSe**, poly(3-hexylthiophene-*alt*-3-hexyltellurophene) **PSTe** and poly(3-hexylselenophene-*alt*-3-hexyltellurophene) **PSeTe** (Fig. 1).[48] Development of a block conjugated polymer where one block is comprised of an alternating copolymer is also of great interest in polymer science. For example, poly[3-hexylthiophene-*block*-(*alt*-donor–acceptor)$_n$], where **P3HT** is the first block followed by covalent extension with the second block of an alternating D–A conjugated copolymer, was designed and synthesized.[49,50] The purpose of such a polymer arrangement is to induce microphase separation between the donor block (**P3HT**) and the acceptor block (D–A) which can be used as a single-component active layer for organic solar cells.[51,52] To the best of our knowledge, block conjugated polymers in which both blocks are constituted by alternating copolymers denoted as poly(*alt*-AB)$_x$-*b*-(*alt*-AC)$_y$ have seldom been reported and explored.[53] We envision that 3-hexylthiophene, 3-hexylselenophene and 3-hexyltellurophene could be used as A, B and C units to create such unprecedented sequence-controlled polychalcogenophenes with high side-chain regioregularity. To this end, we report the first synthesis of a new class of poly(*alt*-AB)$_x$-*b*-(*alt*-AC)$_y$ type polychalcogenophenes where each block consists of an alternating copolymer, including poly(3-hexylthiophene-*alt*-3-hexylselenophene)-*block*-(3-hexylthiophene-*alt*-3-hexyltellurophene) denoted as **P(SSe)*b*(STe)**, poly(3-hexylthiophene-*alt*-3-hexylselenophene)-*block*-(3-hexylselenophene-*alt*-3-hexyltellurophene) denoted as **P(SSe)*b*(SeTe)** and poly(3-hexylthiophene-*alt*-3-hexyltellurophene)-*block*-(3-hexylselenophene-*alt*-3-hexyltellurophene) denoted as **P(STe)*b*(SeTe)** (Fig. 1). Their structural features, intrinsic molecular and morphological properties, Br_2 oxidation and OFETs for Br_2 sensors have been thoroughly investigated.

Results and discussion

Synthesis of block copolymer

The block copolymers were synthesized *via* Grignard metathesis followed by Kumada catalyst transfer polycondensation (KCTP). Three kinds of unsymmetrical diiodobichalcogenophene

Open Access Article. Published on 14 July 2023. Downloaded on 2/13/2026 6:50:17 PM. This article is licensed under a Creative Commons Attribution-NonCommercial 3.0 Unported Licence.

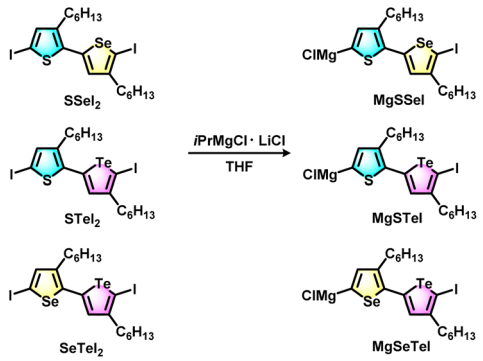

Scheme 1 Regioselective Grignard metathesis of $SSeI_2$, $STeI_2$, and $SeTeI_2$ monomers with ^{i}PrMgCl·LiCl to form unsymmetrical active monomer species MgSSeI, MgSTeI, and MgSeTeI.

monomers $SSeI_2$, $STeI_2$, and $SeTeI_2$ were designed and synthesized according to our previous work.[48] Due to the favorable electronic and steric effects, the Grignard metathesis of $SSeI_2$, $STeI_2$, and $SeTeI_2$ with one equivalent of ^{i}PrMgCl·LiCl occurs regioselectively at the lighter chalcogenophenes to form MgSSeI, MgSTeI, and MgSeTeI, respectively (Scheme 1).

For the synthesis of **P(SSe)*b*(STe)**, the $SSeI_2$ was reacted with ^{i}PrMgCl·LiCl to form MgSSeI which undergoes Ni(dppp)Cl_2-catalyzed Kumada polymerization at room temperature. After the MgSSeI monomer was completely consumed to form the first **PSSe** block for 30 min, a second freshly prepared MgSTeI monomer was introduced to continue elongating the second block for 2 h, leading to the formation of **P(SSe)*b*(STe)**. The molar ratio of Ni(dppp)Cl_2/MgSSeI/MgSTeI is set as 1 : 50 : 50. High-temperature gel permeation chromatography with trichlorobenzene as eluent was used to monitor the polymerization reaction. As soon as the polymerization was quenched by 6 M HCl/MeOH solution after 30 min, the molecular weight of the first block **PSSe** was determined to be M_n = 11.4 kDa with a dispersity ($Đ$) of 1.20 (Fig. 2). The resultant block polymer **P(SSe)*b*(STe)** exhibited an increased M_n = 24.2 kDa with $Đ$ = 1.30, confirming the continuous growth of the second **PSTe** block on the first **PSSe** block.

In a similar manner, **P(SSe)*b*(SeTe)** and **P(STe)*b*(SeTe)** were successfully prepared by Grignard metathesis/Kumada Ni(dppp)Cl_2-catalyzed sequence-controlled polymerization of MgSSeI (first block, 30 min)/MgSeTeI (second block, 2 h) and MgSTeI (first block, 30 min)/MgSeTeI (second block, 2 h), respectively (Fig. 2). The molecular weights of the first block and block polymers are shown in Fig. 2. Because the molar ratio of Ni(dppp)Cl_2/first monomer/second monomer is kept as 1 : 50 : 50, the conjugated length of the two blocks in the three polymers is approximately the same due to the CTP character. As

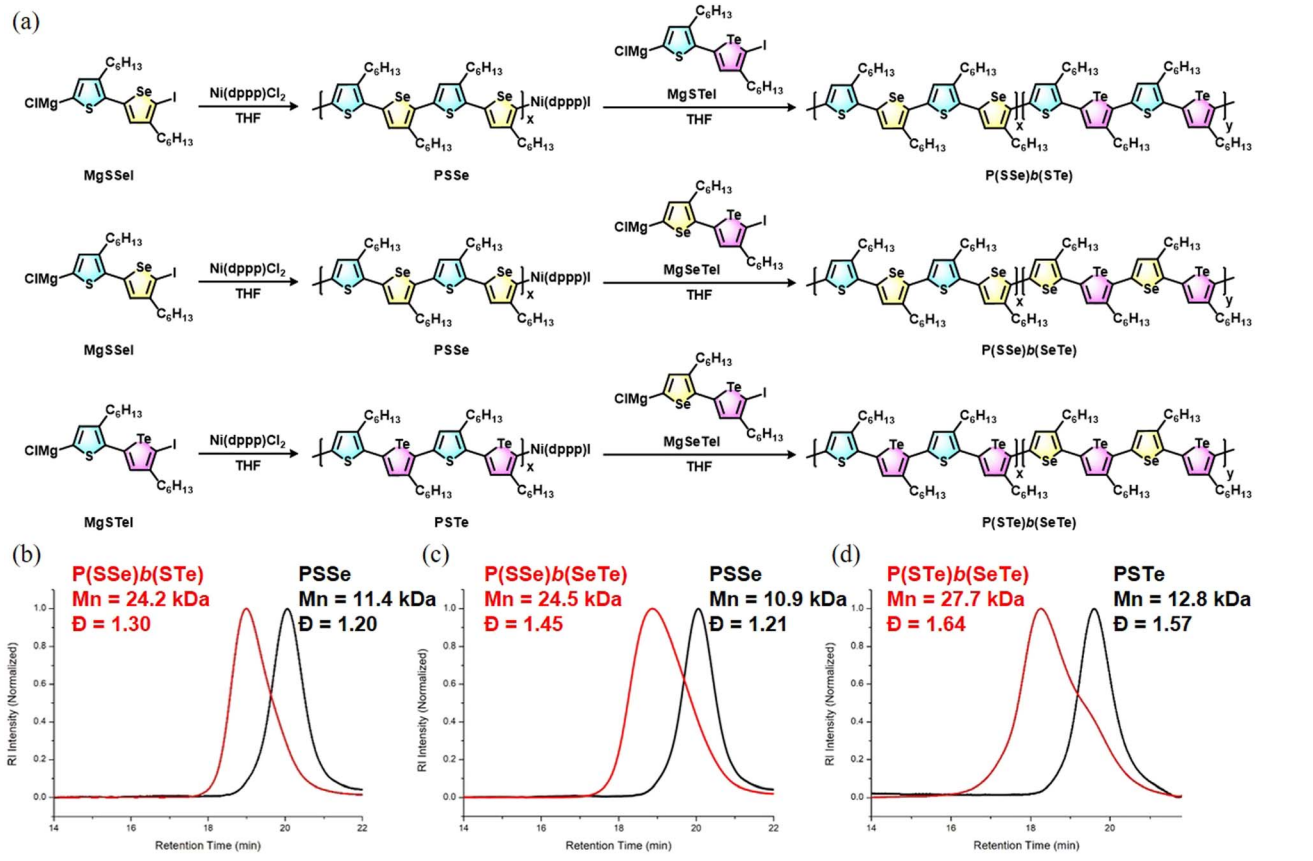

Fig. 2 (a) Synthesis of alternating block copolymers **P(SSe)*b*(STe)**, **P(SSe)*b*(SeTe)** and **P(STe)*b*(SeTe)** by two-step sequential Ni(dppp)Cl_2-catalyzed Kumada polymerization; GPC curves with molecular weight and dispersity for (b) **PSSe**/**P(SSe)*b*(STe)**, (c) **PSSe**/**P(SSe)*b*(SeTe)**, and (d) **PSTe**/**P(STe)*b*(SeTe)**.

© 2023 The Author(s). Published by the Royal Society of Chemistry

Open Access Article. Published on 14 July 2023. Downloaded on 2/13/2026 6:50:17 PM.
This article is licensed under a Creative Commons Attribution-NonCommercial 3.0 Unported Licence.

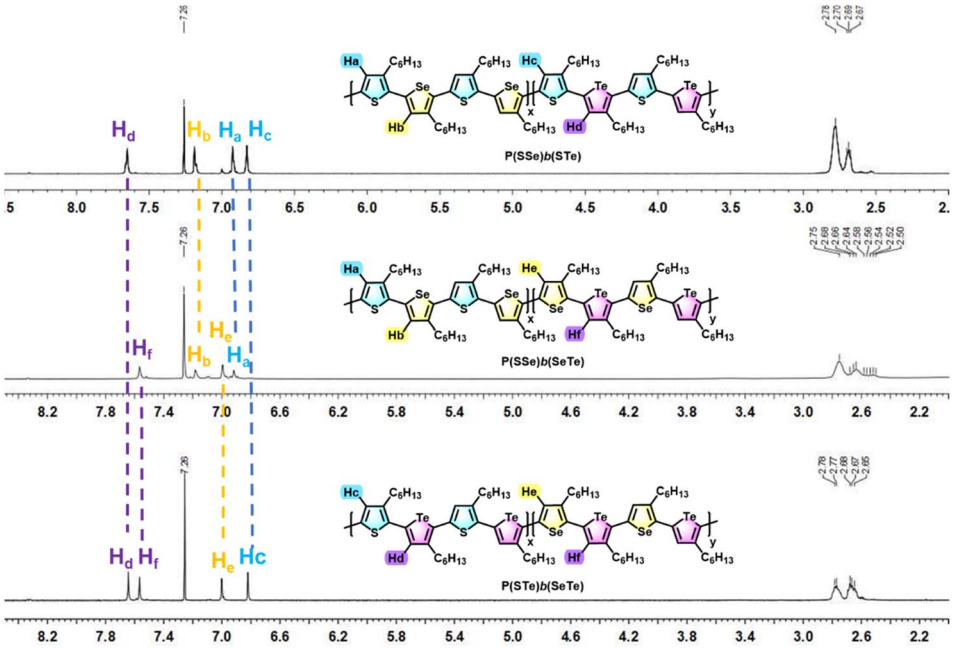

Fig. 3 Comparison of the aromatic protons of **P(SSe)*b*(STe)**, **P(SSe)*b*(SeTe)** and **P(STe)*b*(SeTe)** in ^{1}H NMR spectra.

a result, the ratio of thiophene/selenophene/tellurophene composition is roughly $S_{50\%}/Se_{25\%}/Te_{25\%}$ for **P(SSe)*b*(STe)**, $S_{25\%}/Se_{50\%}/Te_{25\%}$ for **P(SSe)*b*(SeTe)**, and $S_{25\%}/Se_{25\%}/Te_{50\%}$ for **P(STe)*b*(SeTe)**.

^{1}H- and ^{13}C-NMR spectroscopy was used to investigate the chemical structures of the three block alternating poly(-bichalcogenophene)s (Fig. 3 and S1†). The ^{1}H-NMR spectra of the **P(SSe)*b*(STe)**, **P(SSe)*b*(SeTe)** and **P(STe)*b*(SeTe)** polymers all showed four well-defined singlet peaks in the aromatic region, confirming four kinds of protons in four different 3-hexylchalcogenophene environments (two from one block and two from the other), which is consistent with the block structures with high side-chain regioregularity. The chemical shifts of protons on thiophene (H_a)/selenophene (H_b) of the **SSe** block and thiophene (H_c)/tellurophene (H_d) of the second **STe** block are determined to be 6.93/7.19 and 6.83/7.65 ppm, respectively, for **P(SSe)*b*(STe)**. In a similar manner, the chemical shifts of protons on thiophene (H_a)/selenophene (H_b) of the **SSe** block and selenophene (H_e)/tellurophene (H_f) of the second **SeTe** block are determined to be 6.92/7.18 and 7.00/7.57 ppm for **P(SSe)*b*(SeTe)**. Furthermore, the chemical shifts of protons on thiophene (H_c)/tellurophene (H_d) of the **STe** block and selenophene (H_e)/tellurophene (H_f) of the second **SeTe** block are 6.82/7.64 and 7.00/7.57 ppm for **P(STe)*b*(SeTe)**. It should be noted that the chemical shifts of the protons of the **SSe**, **STe** and **SeTe** blocks in the three different polymers are essentially identical, clearly demonstrating the formation of regioregular alternating block architectures. On the other hand, the integration ratio of $H_a + H_b : H_c + H_d$ for **P(SSe)*b*(STe)**, $H_a + H_b : H_e + H_f$ for **P(SSe)*b*(SeTe)** and $H_c + H_d : H_e + H_f$ for **P(STe)*b*(SeTe)** is approximately

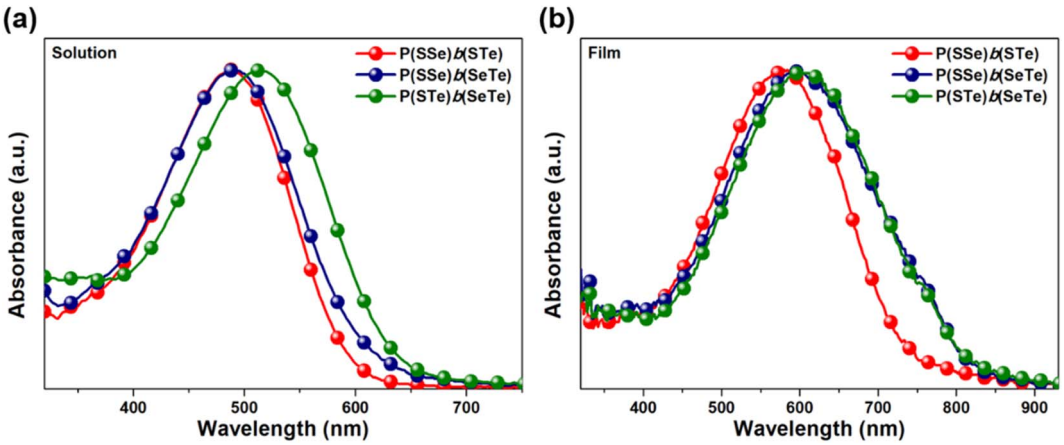

Fig. 4 Absorption spectra of **P(SSe)*b*(STe)**, **P(SSe)*b*(SeTe)**, and **P(STe)*b*(SeTe)** in (a) *o*-DCB solution and (b) the thin-film state.

Open Access Article. Published on 14 July 2023. Downloaded on 2/13/2026 6:50:17 PM. This article is licensed under a Creative Commons Attribution-NonCommercial 3.0 Unported Licence.

1.00 : 1.01, 1.00 : 1.04 and 1.00 : 1.00, respectively, indicating that the two blocks in the three polymers have essentially the same conjugated length. In other words, the molar ratio of the thiophene : selenophene : tellurophene units in **P(SSe)*b*(STe)**, **P(SSe)*b*(SeTe)** and **P(STe)*b*(SeTe)** is 2 : 1 : 1, 1 : 2 : 1 and 1 : 1 : 2, respectively. This result confirms the character of catalyst transfer polymerization so that the length of the two blocks can be synthetically controlled by the feed ratio of the two monomers (1 to 1). On the other hand, the ^{13}C-NMR spectra of the **P(SSe)*b*(STe)**, **P(SSe)*b*(SeTe)** and **P(STe)*b*(SeTe)** show sixteen aromatic peaks derived from four different 3-hexylchalcogenophene environments, which is also in good agreement with the block structures of the polymers (see the ESI†). The peaks appearing at 2.6–2.8 ppm come from the protons on the first carbon atoms of the hexyl side-chains.

Reversing the synthetic sequence of the block copolymer was also attempted. Using MgSeTeI as the first monomer and MgSSeI as the second monomer resulted in the formation of **P(SeTe)*b*(SSe)** with $M_n = 25.4$ kDa and $Đ = 1.37$ which have the same characteristics as **P(SSe)*b*(SeTe)**. This experiment revealed that changing the monomer addition sequence does not affect the polymerization. The Ni species can undergo reductive elimination to form the carbon–carbon bond at the block–block junction and subsequently migrate (ring walk) to the chain end to propagate the second block.

Optical properties

To investigate the chalcogen effects on the optical absorption behavior of the block polychalcogenophenes, the UV-visible absorption spectra were recorded both in solution state (Fig. 4a) and thin-film state (Fig. 4b). The absorption data are summarized in Table 1. Upon increasing the amount of heavier chalcogenophenes (selenophene and tellurophene) in the polymers, the absorption is gradually red-shifted with accompanying broadening of the full width at half maximum (FWHM) of the band. In solution, the λ_{max} of the **P(SSe)*b*(STe)** block copolymer was observed at 488 nm which is in between those of the **PSSe** (471 nm) and **PSTe** (504 nm). Similarly, the absorption maximum of **P(SSe)*b*(SeTe)** at 490 nm is also in between those of **PSSe** (471 nm) and **PSeTe** (541 nm). With a heavier chalcogen involved, **P(STe)*b*(SeTe)** ($S_{25\%}/Se_{25\%}/Te_{50\%}$) exhibited a strong absorption peak in the 400–600 nm range, extending the λ_{max} to 514 nm (in between **PSTe** and **PSeTe**) as shown in Fig. 4a. All three polymers exhibited red-shifted absorption profiles both in λ_{max} and λ_{onset} values in thin-film states: 584 and 743 nm for **P(SSe)*b*(STe)** ($S_{50\%}/Se_{25\%}/Te_{25\%}$); 594 and 830 nm for **P(SSe)*b*(SeTe)** ($S_{25\%}/Se_{50\%}/Te_{25\%}$); 600 and 830 nm for **P(STe)*b*(SeTe)** ($S_{25\%}/Se_{25\%}/Te_{50\%}$). It is interesting to find that block alternating copolymers **P(SSe)*b*(STe)** ($S_{50\%}/Se_{25\%}/Te_{25\%}$), **P(SSe)*b*(SeTe)** ($S_{25\%}/Se_{50\%}/Te_{25\%}$), and **P(STe)*b*(SeTe)** ($S_{25\%}/Se_{25\%}/Te_{50\%}$) turn out to have more red-shifted λ_{max} values than the single block of alternating copolymers **PSTe** ($S_{50\%}/Te_{50\%}$, 576 nm) and **PSeTe** ($Se_{50\%}/Te_{50\%}$, 589 nm) which actually contain a higher percentage of heavier chalcogenophenes. This result implies that block alternating copolymers might have more ordered π–π stacking than the single block alternating copolymers. In particular, **P(SSe)*b*(SeTe)** showed the most red-shifted λ_{max} from solution to solid state (more than 100 nm shift), implying that **P(SSe)*b*(SeTe)** might have the highest order of polymeric packing among the three polymers. We envisage that the **SSe** block in one **P(SSe)*b*(SeTe)** polymer might prefer to interact with the **SeTe** block in another polymer to form a more balanced π-stacking distance.

Electrochemical properties

Cyclic voltammetry (CV) was evaluated to examine the electrochemical properties of the polymers and determine their HOMO and LUMO energy levels and electrochemical bandgaps (Fig. 5 and Table 1). Increasing the amount of heavier chalcogenophenes in the polymers resulted in the gradually elevated HOMO levels and reduced LUMO levels, thereby narrowing the band gaps, which is consistent with the optical properties.

To gain insight into the molecular orientation and packing of polymers, grazing incidence wide-angle X-ray scattering (GIWAXS) was performed to investigate the morphology of thin films prepared on silicon wafers. The 2D GIWAXS images and the corresponding 1-dimensional out-of-plane (q_z) and in-plane (q_{xy}) diffraction patterns of the polymer thin films annealed at 100 °C for 10 minutes and as-cast are illustrated in Fig. 6 and Table 2, respectively. The polymers exhibited obvious (010) in-plane peaks corresponding to periodic π–π stacking between the two facing conjugated backbones, indicating that the polymers are arranged in predominantly edge-on orientations with the backbone plane nearly perpendicular to the substrate, which is beneficial for horizontal charge transfer.[54,55] The π–π stacking distances (d_π) of **P(SSe)*b*(STe)** and **P(SSe)*b*(SeTe)** showed the same packing distance of 3.84 Å similar to that of lighter block **PSSe** while the d_π of 3.92 Å for the **P(STe)*b*(SeTe)** is between those of the two blocks **PSTe** and **PSeTe** (3.87 Å for **PSeTe**, and 3.94 Å for **PSTe**). Besides, the **P(SSe)*b*(STe)**, **P(SSe)**

Table 1 Optical and electrochemical properties of P(SSe)*b*(STe), P(SSe)*b*(SeTe), and P(STe)*b*(SeTe)

	λ_{max} (nm)						
	o-DCB[a]	Film	λ_{onset} (nm)	E_g^{opt} (eV)	LUMO (eV)	HOMO (eV)	E_g^{ele} (eV)
P(SSe)*b*(STe)	488	584	743	1.67	−2.70	−4.88	2.18
P(SSe)*b*(SeTe)	490	594	830	1.55	−2.71	−4.83	2.12
P(STe)*b*(SeTe)	514	600	830	1.55	−2.86	−4.81	2.01

[a] *O*-dichlorobenzene.

© 2023 The Author(s). Published by the Royal Society of Chemistry

Open Access Article. Published on 14 July 2023. Downloaded on 2/13/2026 6:50:17 PM.
This article is licensed under a Creative Commons Attribution-NonCommercial 3.0 Unported Licence.

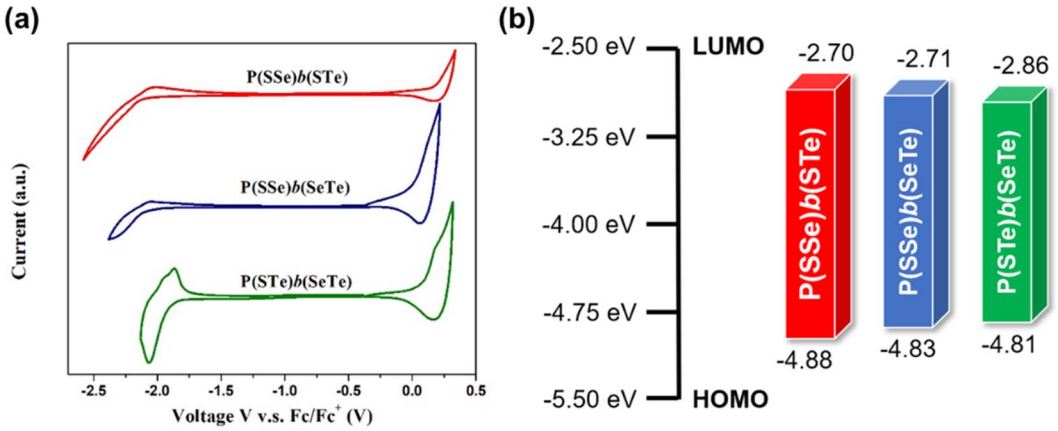

Fig. 5 (a) Cyclic voltammetry plots of **P(SSe)*b*(STe)**, **P(SSe)*b*(SeTe)**, and **P(STe)*b*(SeTe)** in thin films and (b) the HOMO/LUMO energy levels.

***b*(SeTe)** and **P(STe)*b*(SeTe)** polymer films exhibited out-of-plane ($h00$) signals assigned to a lamellar spacing (d_l) corresponding to side-chain interdigitation. Interestingly, the lamellar spacing d_l decreased upon increasing the tellurophene content (16.02 Å for **P(STe)*b*(SeTe)**, 16.08 Å for **P(SSe)*b*(STe)**, and 16.44 Å for **P(SSe)*b*(SeTe)**). This observation can be rationalized by the fact that the increased π–π stacking distance allows more space for the interdigitation of hexyl groups, thus leading to the shortened lamellar distance.[56,57] After thermal annealing at 100 °C for 10 min, the d_π distance of **P(SSe)*b*(STe)** and **P(SSe)*b*(SeTe)** slightly decreases with enhanced signal intensities, indicating the thermal-induced formation of more compact structures.

Morphological characterization

Atomic force microscopy (AFM) was conducted to investigate the surface morphology of the block copolymers in the thin film state (Fig. 7). Because of the relatively low solubility of the polymers, *o*-dichlorobenzene was chosen as the processing solvent. The root-mean-square roughness (R_q) is associated with the content of chalcogenophene units. **P(SSe)*b*(STe)** ($S_{50\%}$/$Se_{25\%}$/$Te_{25\%}$) with 50% thiophene content exhibited a relatively smooth and uniform surface with a small root-mean-square roughness (R_q) of 1.88 nm. The R_q of **P(SSe)*b*(SeTe)** ($S_{25\%}$/$Se_{50\%}$/$Te_{25\%}$) and **P(STe)*b*(SeTe)** ($S_{25\%}$/$Se_{25\%}$/$Te_{50\%}$) with increasing heavier chalcogenophene content is increased to

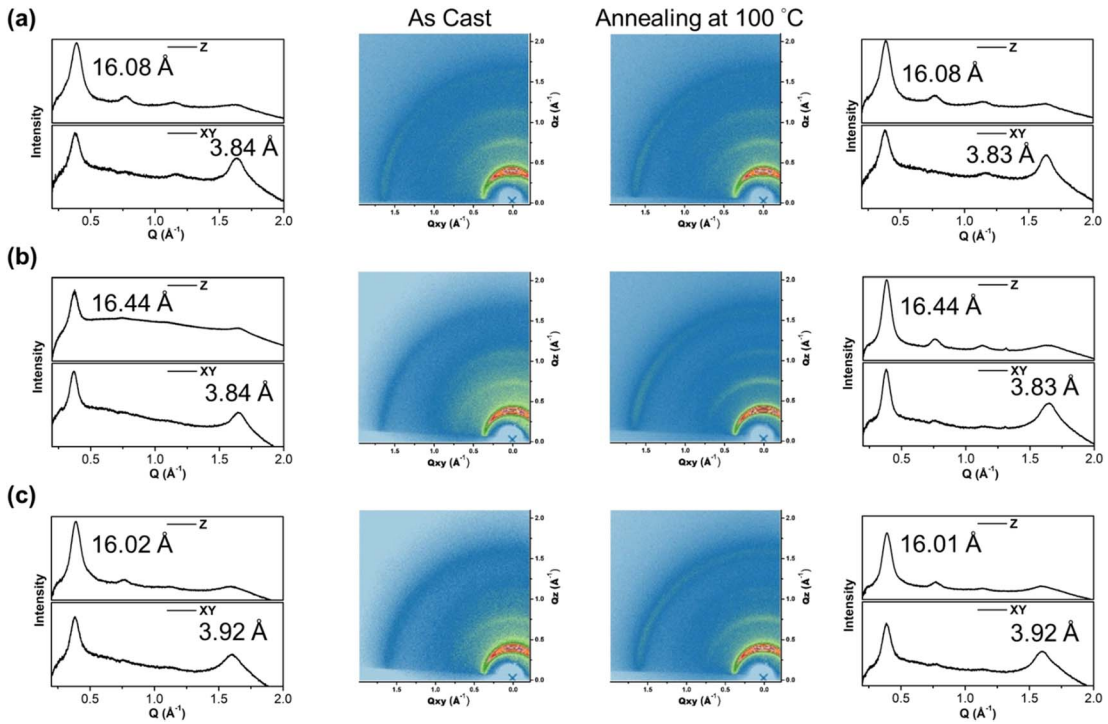

Fig. 6 (a) **P(SSe)*b*(STe)**, (b) **P(SSe)*b*(SeTe)**, and (c) **P(STe)*b*(SeTe)** 2D-GIWAXS images of the polymer thin films measured before and after thermal annealing at 100 °C and their corresponding 1D in-plane (bottom) and out-of-plane (up) linecuts.

Open Access Article. Published on 14 July 2023. Downloaded on 2/13/2026 6:50:17 PM. This article is licensed under a Creative Commons Attribution-NonCommercial 3.0 Unported Licence.

Table 2 Lamellar and π-stacking spacings of the polymers

	As-cast		After thermal annealing at 100 °C	
	Lamellar spacing (d_l) (Å)	π-Stacking spacing (d_π) (Å)	Lamellar spacing (d_l) (Å)	π-Stacking spacing (d_π) (Å)
P(SSe)*b*(STe)	16.08	3.84	16.08	3.83
P(SSe)*b*(SeTe)	16.44	3.84	16.44	3.83
P(STe)*b*(SeTe)	16.02	3.92	16.01	3.92
PSSe	16.51	3.84	16.51	3.83
PSTe	15.95	3.94	15.92	3.92
PSeTe	16.33	3.87	16.28	3.87

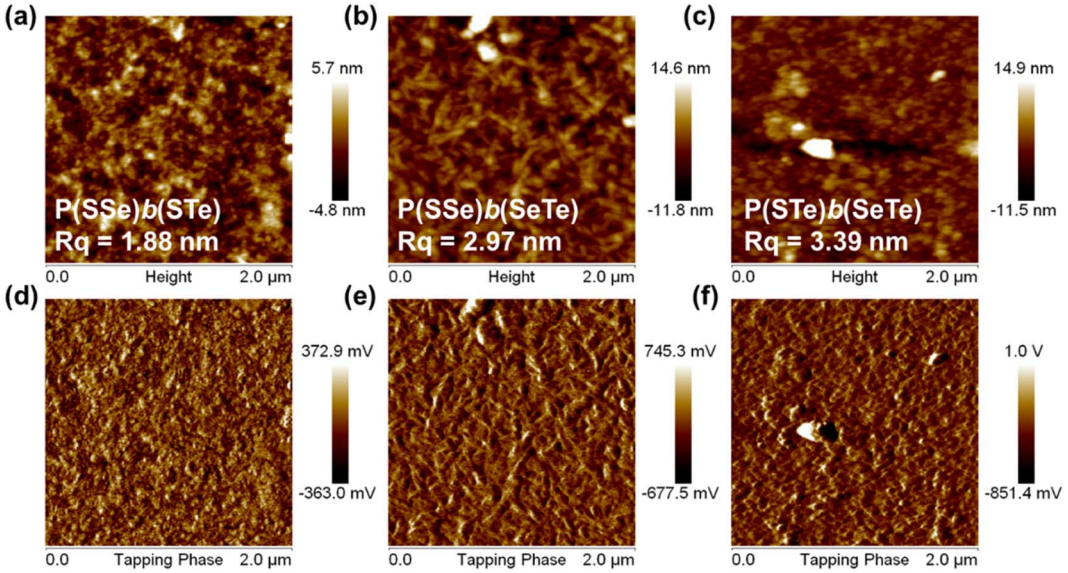

Fig. 7 Height (a–c) and phase (d–f) images of atomic force microscopy: **P(SSe)*b*(STe)** (a and d), **P(SSe)*b*(SeTe)** (b and e), and **P(STe)*b*(SeTe)** (c and f).

2.97 and 3.39 nm, respectively. As the ratio of heavier chalcogenophenes increases in a polymer, the strength of intermolecular interaction also increases. These changes lead to the formation of larger aggregates with higher R_q.

Transistor characterization

To investigate the charge mobility of three p-type polymers, organic field-effect transistors (OFETs) were fabricated by spin-coating **P(SSe)*b*(STe)**, **P(SSe)*b*(SeTe)** and **P(STe)*b*(SeTe)** solutions on the incorporating ODTS-treated SiO_2/Si dielectric substrates in a bottom-gate/top-contact structure. The polymeric thin films were thermally annealed at 100 °C for 10 min. The output characteristics and transfer characteristics are shown in Fig. 8. Due to the edge-on π–π stacking orientation for efficient charge transport in OFETs, **P(SSe)*b*(STe)** exhibited a hole mobility of 1.4×10^{-2} cm^2 V^{-1} s^{-1}, which represents one of the highest values among the tellurophene-containing polychalcogenophenes. It is also interesting to find that the mobility of block **P(SSe)*b*(STe)** is higher than that of the single block polymer (7.2×10^{-3} cm^2 V^{-1} s^{-1} for **PSSe** and 2.7×10^{-3} cm^2 V^{-1} s^{-1} for **PSTe**) due to further reduced packing distances.

While introducing heavier chalcogenophenes, **P(SSe)*b*(SeTe)** and **P(STe)*b*(SeTe)** exhibited slightly reduced mobilities of 5.0×10^{-3} cm^2 V^{-1} s^{-1} and 4.6×10^{-3} cm^2 V^{-1} s^{-1}. Similarly, the values are also higher than that of single block **PSeTe** (5.2×10^{-4} cm^2 V^{-1} s^{-1}).

In particular, **P(STe)*b*(SeTe)** containing 50% Te has larger π–π stacking spacing (3.92 Å) due to the larger radius of the Te atom, which might affect the intermolecular charge hopping transportation. Moreover, **P(SSe)*b*(SeTe)** and **P(STe)*b*(SeTe)** exhibit relatively low solubility due to the presence of strong Te–Te, Se–Se, or Te–Se interactions. This characteristic poses a challenge in forming high-quality thin films suitable for OFETs. We envisage that the OFET mobility of tellurophene-containing polychalcogenophenes can be improved by replacing the hexyl group with longer branched aliphatic side chains.

Bromine addition for PSTe and P(SSe)*b*(PSTe)

The metalloid character of tellurium enables tellurophene to undergo chemical coordination to form hyper-valence species.[58–61] In particular, previous studies conducted by Seferos *et al.* and others have demonstrated that small molecules and

© 2023 The Author(s). Published by the Royal Society of Chemistry

Open Access Article. Published on 14 July 2023. Downloaded on 2/13/2026 6:50:17 PM. This article is licensed under a Creative Commons Attribution-NonCommercial 3.0 Unported Licence.

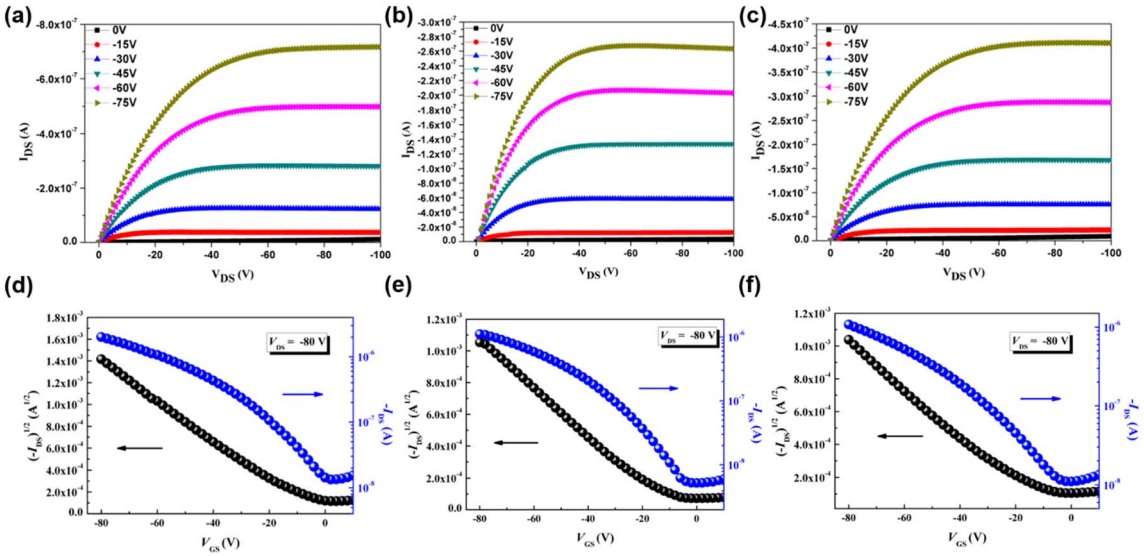

Fig. 8 Output and transfer characteristics of OFETs based on **P(SSe)*b*(STe)** (a and d), **P(SSe)*b*(SeTe)** (b and e), and **P(STe)*b*(SeTe)** (c and f).

conjugated polymers incorporating tellurophene units can undergo bromine addition at the tellurium (Te) center.[62–67] However, bromine addition for tellurophene-incorporated polychalcogenophenes in an alternating fashion and the resulting properties have never been explored. **$STePh_2$**, a monomer containing a single (3-hexylthiophene-3-

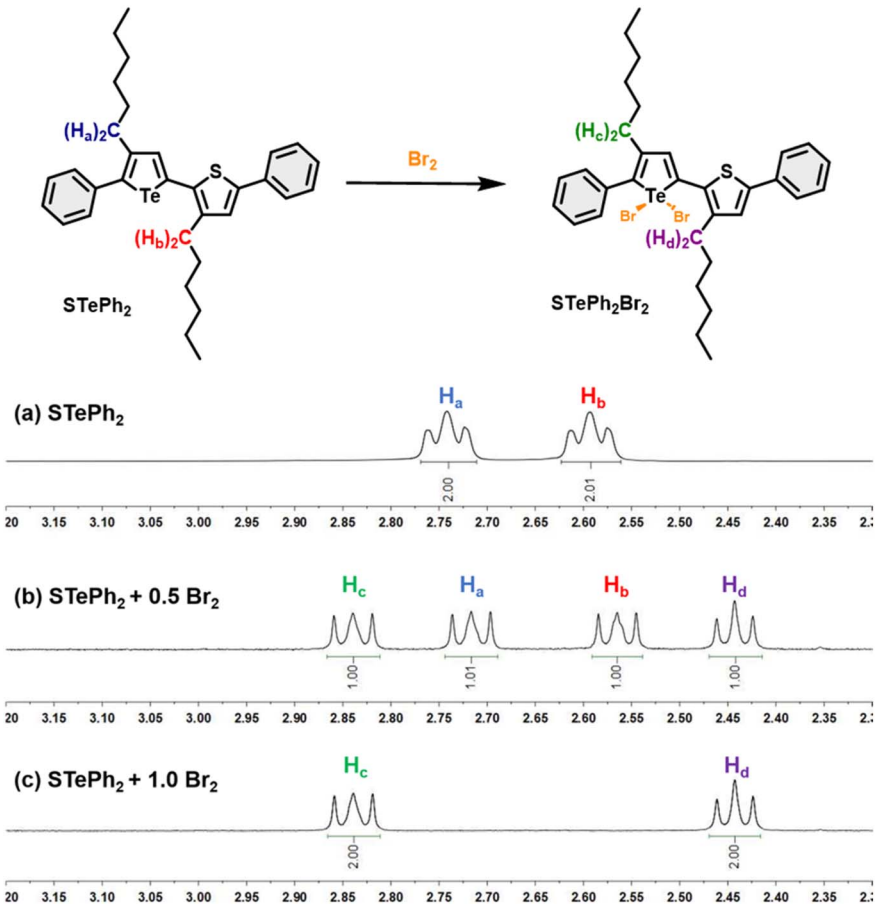

Fig. 9 Bromine addition for the **$STePh_2$** model compound. ^{1}H NMR spectra of (a) **$STePh_2$** and (b) **$STePh_2$** with 0.5 eq. of Br_2 and (c) **$STePh_2$** with 1 eq. of Br_2 in the aliphatic region (2.3–3.2 ppm). H_a/H_b are protons on the alpha carbons of the hexyl groups in **$STePh_2$** and H_c/H_d are the corresponding protons in **$STePh_2Br_2$** after bromination.

Open Access Article. Published on 14 July 2023. Downloaded on 2/13/2026 6:50:17 PM. This article is licensed under a Creative Commons Attribution-NonCommercial 3.0 Unported Licence.

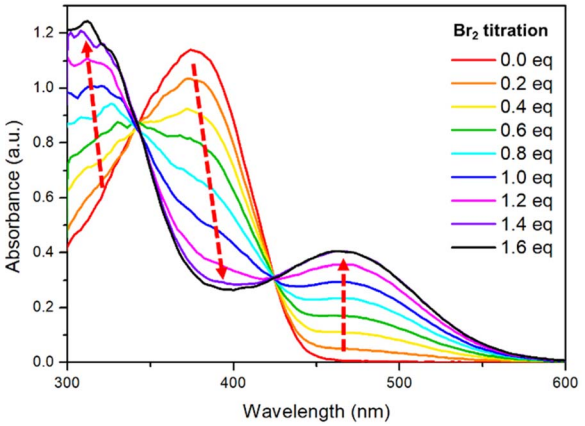

Fig. 10 Absorption spectra of $STePh_2$ in $CHCl_3$ upon bromine titration.

hexyltellurophene) unit, was designed and synthesized as a reference compound for carefully studying the bromine coordination (Fig. 9 and S2†). ^{1}H-NMR of **$STePh_2$** is used to monitored the progress of bromine addition. The two triplet peaks at around 2.5–3.0 ppm are from the characteristic protons of the first carbon (CH_2) in the two different hexyl groups (Fig. 9). Upon titration of 0.5 eq. of bromine in the solution, two new triplet peaks emerge and the integration ratio between the original and new triplet peaks is about 1 : 1, implying that 50% of **$STePh_2$** undergoes bromine addition at the tellurophene moiety. Upon titration of 1 eq. of bromine in the solution, the original peaks are completely replaced by the new triplet peaks. Similar behaviors can be observed in the aromatic region, ruling out the possibility of bromo-substitution at the β-position of thiophene or tellurophene. The absorption spectrum of **$STePh_2$** was also measured upon addition of bromine (Fig. 10). The absorption band with λ_{max} at 376 nm is gradually decreased with concomitant appearance of a new band at 462 nm. The absorption profile is saturated when 1.4 eq. of bromine is introduced. The observation of an isosbestic point at 425 nm clearly indicates that only two **$STePh_2$** and **$STePh_2Br_2$** species are directly interconverted without formation of other intermediates. Mass spectrometry showing the molecular weight of 742 *m*/*z* again confirms the formation of **$STePh_2Br_2$** (Fig. S3†).

After the structure of **$STePh_2Br_2$** has been confirmed, we further monitor the absorption change of the alternating **PSTe** copolymer with 50% of tellurophene with respect to bromine addition. To be more precise, for titration, the concentration of **PSTe** (M) in *o*-DCB is calculated based on the molecular weight of the **STe** repeating unit (428.15 *m*/*z*). When bromine (from low to high: 0.2, 0.4, 0.6, 0.8, 1.0, 1.2, 1.4, 1.6, 1.8, and 2.0 equivalents) is introduced, the λ_{max} band at 504 nm is gradually reduced and hypsochromically shifted while a new band at longer wavelengths steadily intensifies along with the bathochromically shifted λ_{max} (Fig. 11a). The absorption spectrum is saturated at 1.8 eq. of bromine with a final λ_{max} located at 768 nm. The overall λ_{max} red-shift of 264 nm, the largest value ever observed in the literature, is rather significant, indicating that strong and efficient photo-induced intramolecular charge transfer takes place between the [thiophene/electron-deficient **$TeBr_2$** (IV)] units in an alternating manner. The same bromine-addition absorption experiments were carried out for **P(SSe)*b*(PSTe)** whose concentration is based on the molecular weight of **SSeSTe** (908 *m*/*z*) on the condition that the **SSe** and **STe** blocks have the same length. **P(SSe)*b*(PSTe)** exhibited similar optical behaviors with conversion of the original band at λ_{max} of 488 nm to a new band at λ_{max} of 769 nm when reaching saturation at 1.8 eq. of bromine addition (Fig. 11b). Although only the **PSTe** block can react with bromine, the overall λ_{max} red-shift of **P(SSe)*b*(PSTe)** is 281 nm which is even larger than that of **PSTe**. Furthermore, unlike **PSTe**, the original band of **P(SSe)*b*(PSTe)** does not completely vanish upon addition of bromine, which should be ascribed to the absorption of the non-Te **PSSe** block. These results demonstrate that the block and alternating arrangement of **P(SSe)*b*(PSTe)** with the coordination nature of Te enable us to precisely modulate the optical absorption from the UV-Vis to near-infrared region. It should be noted that after bromine addition, the solubility of the **P(SSe)*b*($STeBr_2$)** decreases, which implies stronger intermolecular interactions ascribed to electrostatic interactions or dipole–dipole interactions induced by the more electron-deficient **$TeBr_2$** (IV) species.

OFET devices as bromine sensors

After understanding the Br_2 coordination ability of the tellurophene-containing polychalcogenophenes, it is envisaged

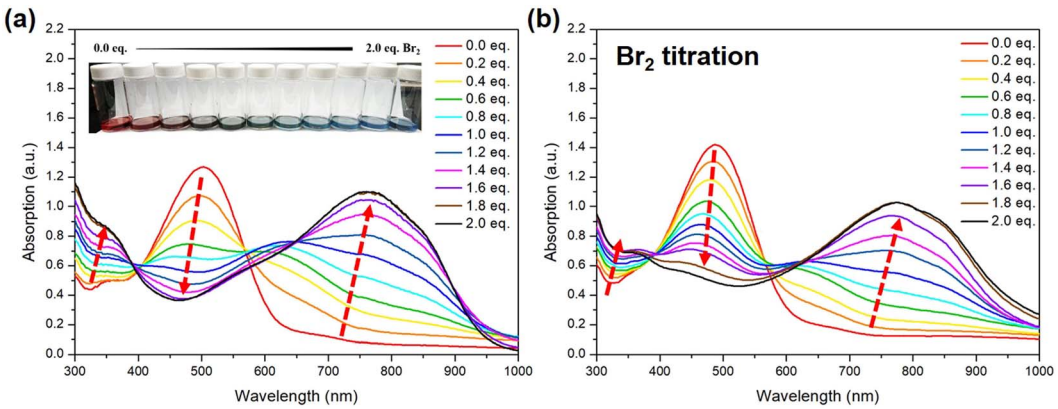

Fig. 11 Absorption spectra of (a) PSTe and (b) P(SSe)*b*(PSTe) in *o*-DCB upon bromine titration.

© 2023 The Author(s). Published by the Royal Society of Chemistry

Open Access Article. Published on 14 July 2023. Downloaded on 2/13/2026 6:50:17 PM.
This article is licensed under a Creative Commons Attribution-NonCommercial 3.0 Unported Licence.

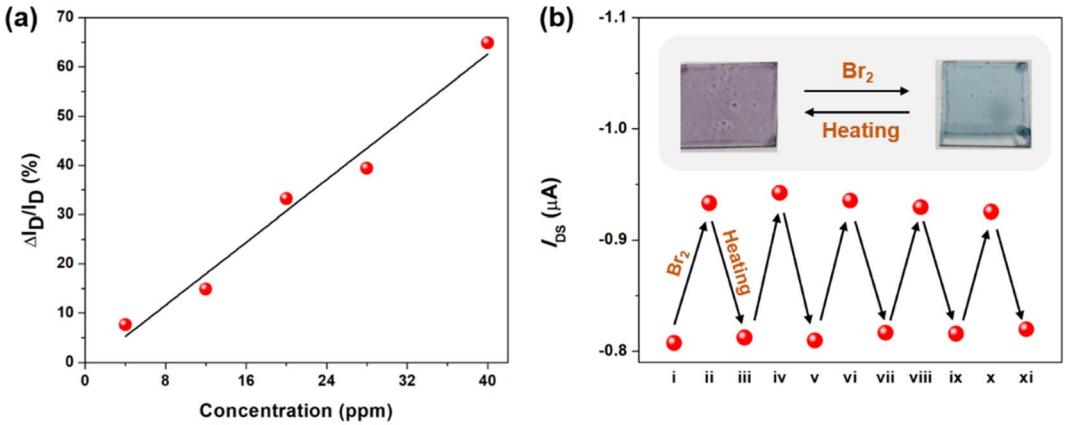

Fig. 12 (a) $\Delta I_{SD}/I_{SD}$ of the **PSTe**-based OFET device as a function of Br_2 vapor concentration. (b) I_{DS} variation of the **PSTe**-OFET device with V_{GS} and V_{DS} at −80 V during five cycles of Br_2 exposure followed by thermal annealing at 150 °C for 10 min.

that OFET devices using these organic semiconducting materials can be utilized for detecting bromine gas. We first fabricated the bottom-gate-top-contact OFET devices made of **PSTe** thin films that exhibited an obvious p-type transistor behavior in the transfer curves to deliver a hole mobility of 2.7×10^{-3} $cm^2\ V^{-1}\ s^{-1}$. After the devices were exposed to Br_2 vapor with different concentration of 4, 12, 20, 28 and 40 ppm, the source-to-drain current (I_{SD}) is steadily increased when the V_{GS} and V_{DS} are kept at −80 V (Fig. S4†). When the surface of the **PSTe** thin film is partially oxidized by Br_2, the oxidized **PSTeBr$_2$** species with electron-deficient character can similarly function as a p-dopant to increase the hole carrier concentration.[68–71] As a result, the magnitude of ΔI_{SD}/pristine I_{SD} (V_{DS} and V_{GS} of −80 V) is linearly proportional to the Br_2 concentration (Fig. 12a). The limit of detection can be extrapolated to be as low as 2.8 ppm. The devices were also exposed to the vapor of common organic solvents including acetone, chloroform, THF, methanol, ethanol, and dichloromethane. None of the devices showed the enhancement of I_{SD}, demonstrating that the devices are only selectively responsive to Br_2 vapor (Fig. S5†). Interestingly, thermal annealing of the brominated **PSTe** thin film at 150 °C for 10 min led to the elimination of the bromine. TGA measurement of the brominated **PSTe** showed a first weight loss of 27% at a temperature of 150 °C, which is consistent with the molecular weight of Br_2 (Fig. S6†). The second weight loss takes place at *ca.* 380 °C which is similar to the T_d of pristine **PSTe**. Furthermore, the absorption spectrum of the **PSTeBr$_2$** thin film completely shifts back to its original profile of **PSTe** after thermal annealing, confirming the thermally induced reduction of the **TeBr$_2$** (IV) species (Fig. S7†). The reversibility between Br_2 addition and elimination endows the Br_2 sensor devices with reusability. After thermal annealing at 150 °C for 10 min, the oxidized polymer in the OFET device is reduced back to the neutral pristine state so that the increased I_{SD} returns back to the original level. As shown in Fig. 12b, the bromination/heating cycle can be applied to the OFET devices repetitively. In a similar manner, the OFET devices using **P(SSe)*b*(STe)**, **P(SSe)*b*(SeTe)**, and **P(STe)*b*(SeTe)** block copolymers can also be used for Br_2 detection (Fig. S8†).

Conclusions

For the first time, we developed a new class of sequence-controlled conjugated polymers denoted as poly(*alt*-AB)$_x$-*b*-(*alt*-AC)$_y$ in which 3-hexylthiophene, 3-hexylselenophene and 3-hexyltellurophene units are used as A, B and C units to assemble three alternating block polychalcogenophenes **P(SSe)*b*(STe)**, **P(SSe)*b*(SeTe)** and **P(STe)*b*(SeTe)**. The block copolymers were prepared by sequential addition of two asymmetrical bichalcogenophene Grignard monomers under the Ni(dppp)Cl_2-catalyzed Kumada polymerization. The molecular weight, dispersity, length of two blocks ($x = y$), side chain regioregularity and main-chain sequence can be synthetically controlled *via* the catalyst transfer polycondensation mechanism. The polymer structures are unambiguously confirmed by ^{1}H-NMR and ^{13}C-NMR spectra. The optical and electrochemical parameters of the polychalcogenophenes can be precisely fine-tuned by the composition and ratio of the different chalcogenophenes. GIWAXS analysis showed that all the polymers exhibited predominantly edge-on orientations. **P(SSe)*b*(STe)** exhibited a hole OFET mobility of 1.4×10^{-2} $cm^2\ V^{-1}\ s^{-1}$, which represents one of the highest values among the tellurophene-containing polychalcogenophenes. The tellurophene units in **PSTe** and **P(SSe)*b*(PSTe)** can undergo Br_2 addition to form the oxidized **TeBr$_2$** species which results in dramatically red-shifted absorption (>280 nm) as a result of the alternating arrangement to induce strong charge transfer character. The OFET devices using these tellurophene-containing polychalcogenophenes as semiconductors can be used for Br_2 detection. The oxidized $TeBr_2$ species on the surface of the OFET device can serve as a p-type dopant to increase the source–drain hole current, showing high sensitivity and selectivity to Br_2. More importantly, the oxidized $TeBr_2$ species in the Br_2 sensors can be thermally reduced back to the neutral state at 150 °C, demonstrating excellent reusability.

Data availability

The details for general measurement and characterization, fabrication of devices, measurements, thermal properties, synthetic procedures, and ^{1}H and ^{13}C NMR spectra are included in the ESI.†

Open Access Article. Published on 14 July 2023. Downloaded on 2/13/2026 6:50:17 PM. This article is licensed under a Creative Commons Attribution-NonCommercial 3.0 Unported Licence.

Author contributions

The project was conceived and conceptualized by Y.-J. Cheng. K.-H. Huang and H.-H. Liu synthesized the polymers and measured all the optical and electrochemical properties and GIWAXS data. K.-Y. Cheng and C.-L. Tsai fabricated the OFETs and analyzed the transistor characterization and bromine sensor experiments. The manuscript was written by K.-H. Huang and Y.-J. Cheng.

Conflicts of interest

There are no conflicts to declare.

Acknowledgements

This work is supported by the National Science and Technology Council, Taiwan (grant no. 110-2628-M-A49-001-MY3 and 111-2221-E-A49-002) and the Center for Emergent Functional Matter Science of National Yang Ming Chiao Tung University from The Featured Areas Research Center Program within the framework of the Higher Education Sprout Project by the Ministry of Education (MOE) in Taiwan. We thank the National Synchrotron Radiation Research Center (NSRRC) in Taiwan, and Prof. U-Ser Jeng and Dr Chun-Jen Su at the BL23A1 station.

References

1 T.-Y. Luh and Y.-J. Cheng, *J. Chin. Chem. Soc.*, 2022, **69**, 1223–1232.
2 J. F. Lutz, M. Ouchi, D. R. Liu and M. Sawamoto, *Science*, 2013, **341**, 1238149.
3 J. Rodriguez, H. H. Dhanjee, B. L. Pentelute and S. L. Buchwald, *J. Am. Chem. Soc.*, 2022, **144**, 11706–11712.
4 C. Xu, C. He, N. Li, S. Yang, Y. Du, K. Matyjaszewski and X. Pan, *Nat. Commun.*, 2021, **12**, 5853.
5 C. Xu, J. Dong, C. He, J. Yun and X. Pan, *Giant*, 2023, **14**, 100154.
6 S. Cheng, R. Zhao and D. S. Seferos, *Acc. Chem. Res.*, 2021, **54**, 4203–4214.
7 M. A. Baker, C.-H. Tsai and K. J. T. Noonan, *Chem.–Eur. J.*, 2018, **24**, 13078–13088.
8 J.-W. Lee, C. Sun, S.-W. Lee, G.-U. Kim, S. Li, C. Wang, T.-S. Kim, Y.-H. Kim and B. J. Kim, *Energy Environ. Sci.*, 2022, **15**, 4672–4685.
9 S. Seo, J.-W. Lee, D. J. Kim, D. Lee, T. N. Phan, J. Park, Z. Tan, S. Cho, T.-S. Kim and B. J. Kim, *Adv. Mater.*, 2023, **35**, e2300230.
10 S. Jung, Y. Cho, Y. Ji, J. Oh, G. Park, W. Kim, S. Jeong, S. M. Lee, S. Chen, Y. Zhang and C. Yang, *Nano Energy*, 2023, **106**, 108059.
11 D. Gao, J. Hollinger, A. A. Jahnke and D. S. Seferos, *J. Mater. Chem. A*, 2014, **2**, 6058–6063.
12 L. R. MacFarlane, H. Shaikh, J. D. Garcia-Hernandez, M. Vespa, T. Fukui and I. Manners, *Nat. Rev. Mater.*, 2020, **6**, 7–26.
13 S. Chen, L. Li, D. Zhai, Y. Yin, X. Shang, B. Ni and J. Peng, *ACS Appl. Mater. Interfaces*, 2020, **12**, 58094–58104.
14 M. Brinkmann and J. C. Wittmann, *Adv. Mater.*, 2006, **18**, 860–863.
15 D.-H. Kim, J.-T. Han, Y.-D. Park, Y. Jang, J.-H. Cho, M. Hwang and K. Cho, *Adv. Mater.*, 2006, **18**, 719–723.
16 Y.-J. Cheng, S.-H. Yang and C.-S. Hsu, *Chem. Rev.*, 2009, **109**, 5868–5923.
17 J.-S. Wu, S.-W. Cheng, Y.-J. Cheng and C.-S. Hsu, *Chem. Soc. Rev.*, 2015, **44**, 1113–1154.
18 S. Ye, V. Lotocki, H. Xu and D. S. Seferos, *Chem. Soc. Rev.*, 2022, **51**, 6442–6474.
19 S. M. Parke, M. P. Boone and E. Rivard, *Chem. Commun.*, 2016, **52**, 9485–9505.
20 J. Hollinger, D. Gao and D. S. Seferos, *Isr. J. Chem.*, 2014, **54**, 440–453.
21 R. S. Ashraf, I. Meager, M. Nikolka, M. Kirkus, M. Planells, B. C. Schroeder, S. Holliday, M. Hurhangee, C. B. Nielsen, H. Sirringhaus and I. McCulloch, *J. Am. Chem. Soc.*, 2015, **137**, 1314–1321.
22 C.-E. Tsai, R.-H. Yu, F.-J. Lin, Y.-Y. Lai, J.-Y. Hsu, S.-W. Cheng, C.-S. Hsu and Y.-J. Cheng, *Chem. Mater.*, 2016, **28**, 5121–5130.
23 F.-Y. Cao, C.-C. Tseng, F.-Y. Lin, Y. Chen, H. Yan and Y.-J. Cheng, *Chem. Mater.*, 2017, **29**, 10045–10052.
24 F.-Y. Cao, F.-Y. Lin, C.-C. Tseng, K.-E. Hung, J.-Y. Hsu, Y.-C. Su and Y.-J. Cheng, *ACS Appl. Mater. Interfaces*, 2019, **11**, 11674–11683.
25 S.-Y. Chen, Y.-C. Pao, S.-K. Sahoo, W.-C. Huang, Y.-Y. Lai and Y.-J. Cheng, *Chem. Commun.*, 2018, **54**, 1517–1520.
26 H.-H. Chang, C.-E. Tsai, Y.-Y. Lai, W.-W. Liang, S.-L. Hsu, C.-S. Hsu and Y.-J. Cheng, *Macromolecules*, 2013, **46**, 7715–7726.
27 S.-Y. Chen, S.-K. Sahoo, C.-L. Huang, T.-H. Chan and Y.-J. Cheng, *Org. Lett.*, 2020, **22**, 2318–2322.
28 E. Rivard, *Chem. Lett.*, 2015, **44**, 730–736.
29 E. I. Carrera and D. S. Seferos, *Macromolecules*, 2014, **48**, 297–308.
30 A. M. Ballantyne, L. Chen, J. Nelson, D. D. C. Bradley, Y. Astuti, A. Maurano, C. G. Shuttle, J. R. Durrant, M. Heeney, W. Duffy and I. McCulloch, *Adv. Mater.*, 2007, **19**, 4544–4547.
31 A. A. Jahnke, B. Djukic, T. M. McCormick, E. Buchaca Domingo, C. Hellmann, Y. Lee and D. S. Seferos, *J. Am. Chem. Soc.*, 2013, **135**, 951–954.
32 M. Heeney, W. Zhang, D. J. Crouch, M. L. Chabinyc, S. Gordeyev, R. Hamilton, S. J. Higgins, I. McCulloch, P. J. Skabara, D. Sparrowe and S. Tierney, *Chem. Commun.*, 2007, 5061–5063.
33 S. Ye, M. Steube, E. I. Carrera and D. S. Seferos, *Macromolecules*, 2016, **49**, 1704–1711.
34 X. Li, P. J. Wolanin, L. R. MacFarlane, R. L. Harniman, J. Qian, O. E. C. Gould, T. G. Dane, J. Rudin, M. J. Cryan, T. Schmaltz, H. Frauenrath, M. A. Winnik, C. F. J. Faul and I. Manners, *Nat. Commun.*, 2017, **8**, 15909.
35 J. Peng and Y. Han, *Giant*, 2020, **4**, 100039.
36 F. Lv, Z. An and P. Wu, *Nat. Commun.*, 2019, **10**, 1397.

© 2023 The Author(s). Published by the Royal Society of Chemistry

Open Access Article. Published on 14 July 2023. Downloaded on 2/13/2026 6:50:17 PM. This article is licensed under a Creative Commons Attribution-NonCommercial 3.0 Unported Licence.

37 X. Lin, S. Ye, C. Kong, K. Webb, C. Yi, S. Zhang, Q. Zhang, J. T. Fourkas and Z. Nie, *J. Am. Chem. Soc.*, 2020, **142**, 17282–17286.
38 J. Hollinger, A. A. Jahnke, N. Coombs and D. S. Seferos, *J. Am. Chem. Soc.*, 2010, **132**, 8546–8547.
39 J. Hollinger, P. M. DiCarmine, D. Karl and D. S. Seferos, *Macromolecules*, 2012, **45**, 3772–3778.
40 J. A. Amonoo, A. Li, G. E. Purdum, M. E. Sykes, B. Huang, E. F. Palermo, A. J. McNeil, M. Shtein, Y.-L. Loo and P. F. Green, *J. Mater. Chem. A*, 2015, **3**, 20174–20184.
41 E. L. Kynaston, Y. Fang, J. G. Manion, N. K. Obhi, J. Y. Howe, D. F. Perepichka and D. S. Seferos, *Angew. Chem., Int. Ed.*, 2017, **56**, 6152–6156.
42 E. L. Kynaston, K. J. Winchell, P. Y. Yee, J. G. Manion, A. D. Hendsbee, Y. Li, S. Huettner, S. H. Tolbert and D. S. Seferos, *ACS Appl. Mater. Interfaces*, 2019, **11**, 7174–7183.
43 M. Zhu, S. Pan, Y. Wang, P. Tang, F. Qiu, Z. Lin and J. Peng, *Angew. Chem., Int. Ed.*, 2018, **57**, 8644–8648.
44 G. E. J. Hicks, C. N. Jarrett-Wilkins, J. R. Panchuk, J. G. Manion and D. S. Seferos, *Chem. Sci.*, 2020, **11**, 6383–6392.
45 Y.-Y. Lai, T.-C. Tung, W.-W. Liang and Y.-J. Cheng, *Macromolecules*, 2015, **48**, 2978–2988.
46 C.-H. Tsai, A. Fortney, Y. Qiu, R. R. Gil, D. Yaron, T. Kowalewski and K. J. T. Noonan, *J. Am. Chem. Soc.*, 2016, **138**, 6798–6804.
47 Y. Qiu, A. Fortney, C.-H. Tsai, M. A. Baker, R. R. Gil, T. Kowalewski and K. J. T. Noonan, *ACS Macro Lett.*, 2016, **5**, 332–336.
48 H.-H. Liu, W.-W. Liang, Y.-Y. Lai, Y.-C. Su, H.-R. Yang, K.-Y. Cheng, S.-C. Huang and Y.-J. Cheng, *Chem. Sci.*, 2020, **11**, 3836–3844.
49 S. Y. Ku, M. A. Brady, N. D. Treat, J. E. Cochran, M. J. Robb, E. J. Kramer, M. L. Chabinyc and C. J. Hawker, *J. Am. Chem. Soc.*, 2012, **134**, 16040–16046.
50 M. Sommer, H. Komber, S. Huettner, R. Mulherin, P. Kohn, N. C. Greenham and W. T. S. Huck, *Macromolecules*, 2012, **45**, 4142–4151.
51 K. Nakabayashi and H. Mori, *Macromolecules*, 2012, **45**, 9618–9625.
52 C. Guo, Y. H. Lin, M. D. Witman, K. A. Smith, C. Wang, A. Hexemer, J. Strzalka, E. D. Gomez and R. Verduzco, *Nano Lett.*, 2013, **13**, 2957–2963.
53 H. Kim, J. Lee, T. Kim, M. Cho and T.-L. Choi, *Angew. Chem., Int. Ed.*, 2022, **61**, e202205828.
54 J. Rivnay, S. C. Mannsfeld, C. E. Miller, A. Salleo and M. F. Toney, *Chem. Rev.*, 2012, **112**, 5488–5519.
55 S. Y. Son, T. Park and W. You, *Chem. Mater.*, 2021, **33**, 4541–4550.
56 L. Li, J. Hollinger, A. A. Jahnke, S. Petrov and D. S. Seferos, *Chem. Sci.*, 2011, **2**, 2306–2310.
57 Y. Wang, H. Cui, M. Zhu, F. Qiu, J. Peng and Z. Lin, *Macromolecules*, 2017, **50**, 9674–9682.
58 T. M. McCormick, A. A. Jahnke, A. J. Lough and D. S. Seferos, *J. Am. Chem. Soc.*, 2012, **134**, 3542–3548.
59 M. Kaur, D.-S. Yang, K. Choi, M.-J. Cho and D.-H. Choi, *Dyes Pigm.*, 2014, **100**, 118–126.
60 G. E. Garrett, G. L. Gibson, R. N. Straus, D. S. Seferos and M. S. Taylor, *J. Am. Chem. Soc.*, 2015, **137**, 4126–4133.
61 K. Wen, L. Wu, X. Wu, Y. Lu, T. Duan, H. Ma, A. Peng, Q. Shi and H. Huang, *Angew. Chem., Int. Ed.*, 2020, **59**, 12756–12761.
62 A. A. Jahnke, G. W. Howe and D. S. Seferos, *Angew. Chem., Int. Ed.*, 2010, **49**, 10140–10144.
63 M. Kaur, D.-S. Yang, J. Shin, T.-W. Lee, K. Choi, M.-J. Cho and D.-H. Choi, *Chem. Commun.*, 2013, **49**, 5495–5497.
64 M. Kaur, D.-H. Lee, D.-S. Yang, H.-A. Um, M.-J. Cho, J.-S. Kang and D.-H. Choi, *Chem. Commun.*, 2014, **50**, 14394–14396.
65 M. Kaur, D.-H. Lee, D.-S. Yang, H.-A. Um, M.-J. Cho, J.-S. Kang and D.-H. Choi, *Dyes Pigm.*, 2015, **123**, 317–322.
66 E. I. Carrera, A. E. Lanterna, A. J. Lough, J. C. Scaiano and D. S. Seferos, *J. Am. Chem. Soc.*, 2016, **138**, 2678–2689.
67 L. Lv, X. Wang, X. Wang, L. Yang, T. Dong, Z. Yang and H. Huang, *ACS Appl. Mater. Interfaces*, 2016, **8**, 34620–34629.
68 B. Yurash, D. X. Cao, V. V. Brus, D. Leifert, M. Wang, A. Dixon, M. Seifrid, A. E. Mansour, D. Lungwitz, T. Liu, P. J. Santiago, K. R. Graham, N. Koch, G. C. Bazan and T. Q. Nguyen, *Nat. Mater.*, 2019, **18**, 1327–1334.
69 E. H. Suh, J. G. Oh, J. Jung, S. H. Noh, T. S. Lee and J. Jang, *Adv. Energy Mater.*, 2020, **10**, 2002521.
70 J. Li, J. Liu and C. Gao, *J. Polym. Sci., Part B: Polym. Phys.*, 2012, **50**, 125–128.
71 J. H. Schön, C. Kloc, E. Bucher and B. Batlogg, *Nature*, 2000, **403**, 408–410.

© 2023 The Author(s). Published by the Royal Society of Chemistry